PAPER • **OPEN ACCESS**

The Effect of the addition of Ta, Zr and in on the corrosion behaviour of CuAlMn alloys prepared via powder metallurgy

To cite this article: Duaa Amer Ali *et al* 2020 *IOP Conf. Ser.: Mater. Sci. Eng.* **987** 012030

IOP Conf. Series: Materials Science and Engineering **987** (2020) 012030 doi:10.1088/1757-899X/987/1/012030

The Effect of the addition of Ta, Zr and in on the corrosion behaviour of CuAlMn alloys prepared via powder metallurgy

Duaa Amer Ali[a], Ali Hubi Haleem[b], Haydar H.J. Jamal Al-Deen[b],

[a] MSc. Materials Engineering, University of Babylon, Iraq.

[b]Department of Metallurgical Engineering, Materials Engineering Faculty, University of Babylon, Iraq.

alialihhhobi@gmail.com, jaberjd@gmail.com, du3a3030@gmail.com

Abstract. CuAlMn-X (X= Ta, Zr and In) shape memory alloy was fabricated using the powder metallurgy (PM) technique. After sintering at 950 °C, the products were processed using two heat treatments (solution heat treatment at 900 °C and aging at 500 °C). The influence of Tantalum (Ta), Zirconium (Zr) and Indium (In) with three wt.% on the mechanicals properties (hardness), corrosion behaviour and microstructure of CuAlMn shape memory alloys was investigated in this paper. The effect of the addition of Ta, Zr and In alloys was investigated using X-rays diffraction (XRD), open circuit potential, electrochemical tests (Tafel extrapolation method) and Vickers micro-hardness. For the corrosion tests, a 3.5 % NaCl (chloride solution) was used as corrosion solution. The results showed that there is an increase in hardness with addition of the alloy element (Ta, Zr and In) and decrease in the size of martensite plate form, as shown in the microstructures. Furthermore, it was found that the corrosion resistance of Cu-Al-Mn after the addition improved, as shown by the increase in the corrosion potential and decrease in the corrosion current densities. The improvement percentage for CuAlMnTa, CuAlMnIn and CuAlMnZr in the corrosion rate was 97 %, 91 % and 77 %, respectively.

Keywords: *Powder metallurgy, CuAlMn alloys. Cu-based memory alloy, Zirconium addition, Tantalum addition, Indium addition*

1. Introduction

Shape memory alloys (SMAs) are intelligent materials that remember their initial shape when they are heated above their transformation temperature (TT). At a lower temperature than the TT, these properties allow these alloys to distort into new shapes. When the alloys are heated higher than the TT, the crystal structure variant causes the material to go back to the preformed shape [1–2]. SMAs have no diffusion, and the first transformation is characterised by an atomic shearing of the crystal lattice from a high to a low temperature, which represents the structural characteristic called martensite variants [3]. Binary system Cu-Al alloys can be utilised for different applications, such as pumps, valves, bushings and bearings [4]. The high damping capacity of SMAs make them good candidates for seismic damping [5].

The advantages of CuAlMn SMAs are that they are economical, strong and have excellent damping limits within their austenitic to martensitic phase transformation compared to other systems as NiTi. Additionally, grain refining the alloy elements to SMAs can influence the TT (increase or decrease) and shape effects and enhance the stress cracking resistance that is produced during quenching [6]. The addition of

manganese (Mn) improved the binding force between atoms, which led to increased diffusion activation energy and a reduced diffusion rate of the atom for re-ordering [7–8].

Powder metallurgy (PM) is a favourable production path, as it provides a net or near shape, is cheap and controls the chemical composition and grain size [9]. The Cu_3Al-essential basis for SMAs has thermos-mechanical characteristics that are related to the shape memory of the SME and super elasticity of the SE. Additional cooling of the Cu_3Al observed these structures form as a body centre cubic (β) → (18R, 9R). The phases that can take place at higher and lower temperatures near the Cu_3Al composition could be determined using the following steps: 1) the disordered β phase (A_2 or body centre cubic structure) is the balanced structure at elevated temperatures, and 2) the balanced phases at low temperatures are the α-Cu, T_3-Cu_3Mn_2Al, γ_2-Cu_9Al_4 and β-Mn phases. The metastabe random body centre cubic (β) phase passes through the following two transition sequences during cooling: beta two structure and DO_3 martensite structure of Cu_3Al or the L_{21} parent phase of the Cu_2AlMn. To summarise the previous phases transformations of the CuAlMn shape memory alloys, the stoichiometric Cu_3Al alloy first $DO_3 \leftrightarrow A_2$ transition is obtained, whereas for concentrations near Cu_2AlMn, the following two second transitions are found: $L_{21} \leftrightarrow B_2$ and $B_2 \leftrightarrow A_2$ [10–15]. The aim of this research is to prepare the CuAlMn SMA using powder metallurgy and investigate the corrosion resistance of CuAlMn SMAs with Ta, Zr and In three % wt. in a 3.5 % NaCl solution.

2. Experimental Section

2.1. **Powders and its Tests**: The purity of the powders was conducted using the laser particle size analyser type Bettersize and a particle size analysis X-ray fluorescent (XRF), as shown in Table 1 and Figure 1.

Table 1: Powder specifications.

Powders	Average particle size (µm)	Purity %	Supplier
Copper	4.827	99.57	India / CDH fined chemical / Central Drug House (P) Ltd.
Aluminium	19.09	99.06	=
Manganese	19.38	99.84	=
Tantalum	11.74	99.86	=
Zirconium	14.23	99.98	=
Indium	18.46	99.2	=

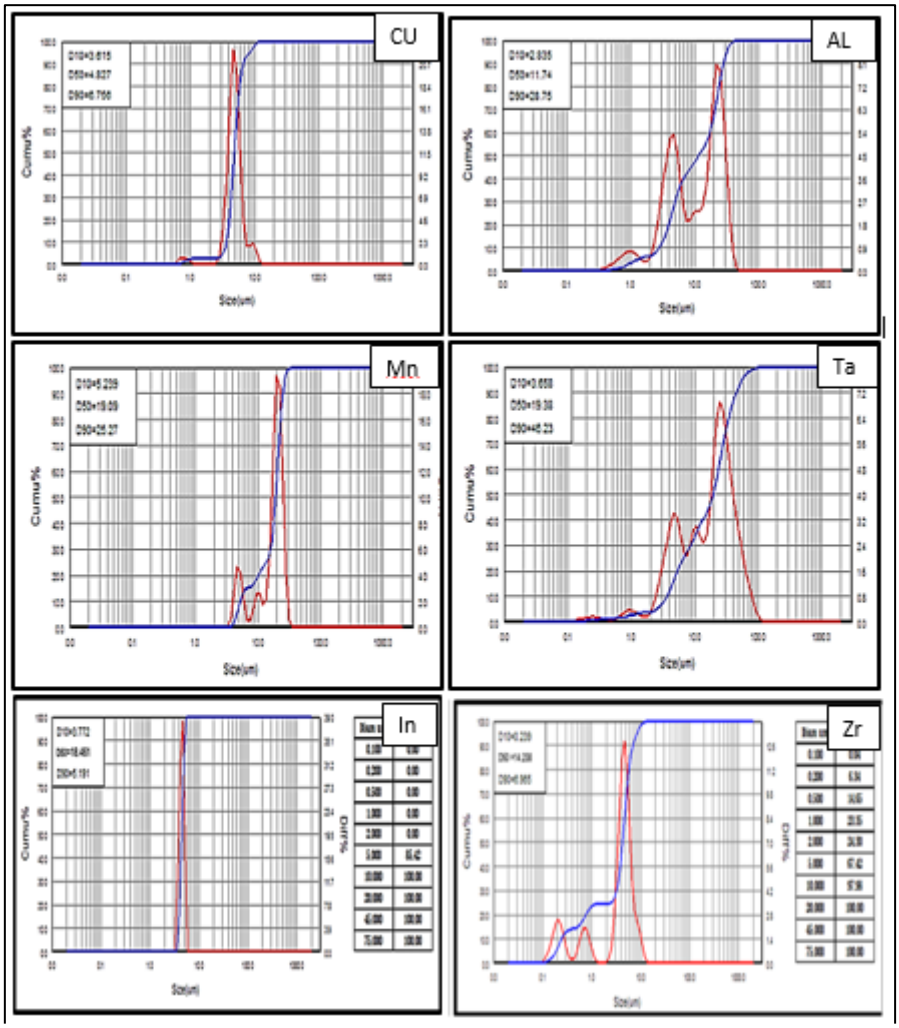

Figure1: Practical size analysis.

2.2. **Preparation of Samples**: The SMAs CuAlMn was prepared using the PM method under an Ar atmosphere to form an ingot. Table 2 shows all samples of CuAlMn and its composites and the percentage of powders in their composition.

Table 2: All samples of CuAlMn and its composites.

Codes	Cu wt.%	Al wt.%	Mn wt.%	Ta wt.%	Zr wt.%	In wt.%
CAM	83	8	9	-	-	-
CAMTa	80	8	9	3	-	-
CAMZr	80	8	9		3	-
CAMIn	80	8	9	-	-	3

The amount of the Cu element varied based on the amount of Ta, Zr and In elements, whereas Al and Mn were kept constant in the alloys. The first-stage powders were mixed in a planetary ball mill for four hours in the presence of ethyl alcohol. Alcohol was added to prevent friction between the mould and powder particles and to reduce the oxidation of the powder particles during the mixing process. During the compacting stage, the mixture was cold compacted in a mould under uni-axial direction using an electric hydraulic press with a compression pressure of nine tons. The dimensions of the mould are shown in Table 3. Cylindrical samples with a diameter of ≈ 12 mm and length of ≈ five mm were produced.

The third stage was sintering, where a heat treatment applied on green was compacted to create bonding between atoms. The sintering furnace consisted of a quartz tube and two ends. One side of the tube was installed into a bottle of water, and the other side was connected to an argon gas cylinder (supply). The other end of tube was connected to a vacuum pump and argon supply. During one sintering process, three specimens were placed into a quartz tube from one end. The samples were placed inside a crucible and submerged into an alumina material crucible. The argon gas pump generated a vacuum atmosphere to prevent oxidation during high temperatures at two bar / min. in quartz tube A. This tube was suspended horizontally into the CARBOLITE tube furnace without touching the wall of the tube furnace. The heating rate of the sintering cycle was set at ten ˚C / min. Figure 2 explains the sintering procedure and final products.

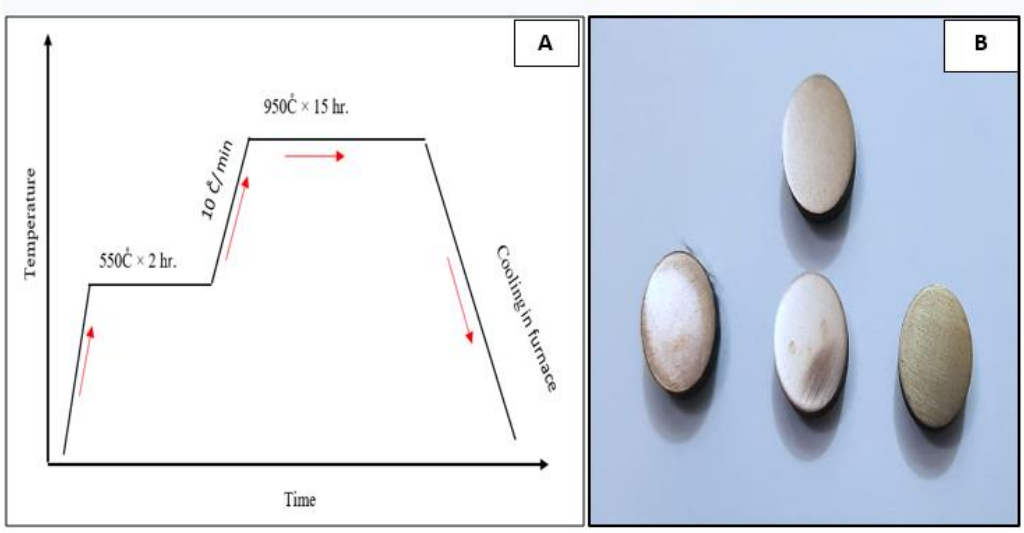

Figure 2: A) sintering heat treatment, B) final production alloys.

2.3. Heat Treatments

Solution heat treatment: the sinter sample is subjected to solution heat treatment, as shown in Figure 3A. The purpose of step quenching is to remove the formation of quench cracks and the pinning of martensitic plates by excess dislocations trapped in quenching from a high temperature. Ageing heat treatment: after the solution heat treatment, the specimens (master alloys with and without additions) were subjected to post-quench isothermal ageing in the austenitic phase. The aging heat treatment cycle is shown in Figure 3B.

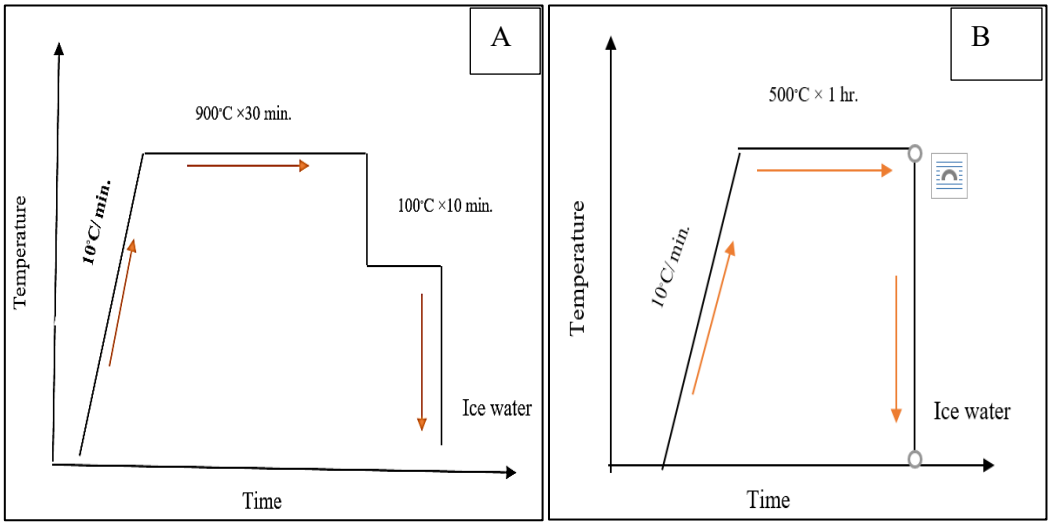

Figure 3: A) solution heat treatment, B) aging heat treatment.

2.4. X-ray diffraction (XRD)

The phases and crystal structures of the alloys were determined using the X-ray diffraction device type shlmadzu XRD-6000 X-Ray diffractometer. The X-Ray diffraction used radiation CuKα with a wavelength of λ = 1.5409 °A 40 kV and 30 mA at room temperature. The diffraction angles (2θ) ranged from 20°–80°.

2.5. Corrosion Test

2.5.1 Open Circuit Potential

Electrochemical investigations were carried out using a three electrode glass cell in 3.5 % NaCl solutions (T = 25 ± one °C). The reference electrode was a saturated calomel electrode, and the counter electrode was a platinum (Pt) electrode.

2.5.2. Electrochemical Tests

Potential-dynamic polarisation was done using a potentiostatic device (winking M lab 200, Germany). The electrochemical cell included specimen alloys that acted as working electrodes. Pt was used as the counter electrode, and the Ag / AgCl electrode was used as a reference electrode. All experiments were conducted at room temperature. The distance between the working and reference electrodes was kept between three to five mm to minimise the ohmic drop across the electrodes. Electrochemical tests were conducted prior to the electrochemical experiments, and each metal sample was grinded and polished to remove the surface oxidation film. The alloys were then degreased ultrasonically for three minutes with ethanol, washed with deionised water and dried. Potentiodynamic polarisation was conducted with a scan rate of + 1.0 mV / s and a start and finish potential of ± 0.25 V vs the open circuit potential (E_{oc}). The corrosion rate (CR) was measured according to Eq. 1 [17–18].

$$CR = 22.85\ I_{corr} \quad \ldots\ldots\ldots\ldots\ldots\ldots\ldots\ldots\ldots\ldots\ldots\ldots\ (1)$$

Where $i$corr is the corrosion's current density.

2.6. Optical Microscope Analysis

The ageing specimens of 12 mm in diameter and four mm in height were ground using SiC paper grits as 180, 400, 800, 1000, 1200 and 2000 then polished using a diamond solution (1 μ). The specimens were etched by ten g $FeCl_3$ + 25 mL HCL + 100 mL distilled water at room temperature. A microscope (1280 XEQMM300TUSB) was used [19].

2.7. Micro-Hardness Measurements

The test was conducted using micro Vickers hardness devices (Digitals Micro Vickers Hardness Tester TH 717) using a load of 500 g for 15 sec with a square-based diamond pyramid.

3. Results and Discussion

3.1. X-ray Diffraction Results

The XRD patterns of CAM SMAs with three different additions of Ta, Zr and In are presented in Figure 4 (A and B) after sintering and aging. It was observed that the formation of phases indicated the formation of both the martensitic and austenite phases. The change in the intensity (I) of the diffraction of the martensite phases peaked based on the limit of the austenite to martensite transformation. Although there was no change observed in the type of martensitic phase with additions, the thickness of the martensite plate decreased, as shown in the OM of the alloys. The results showed that the microstructures of the alloys consist of β̂ and γ` martensites. In these graphs, it is possible to verify the presence of three % Zr, the Cu_5 and Zr phases and Ta_2Al_3 when the addition of Ta was determined [20–21] and [27].

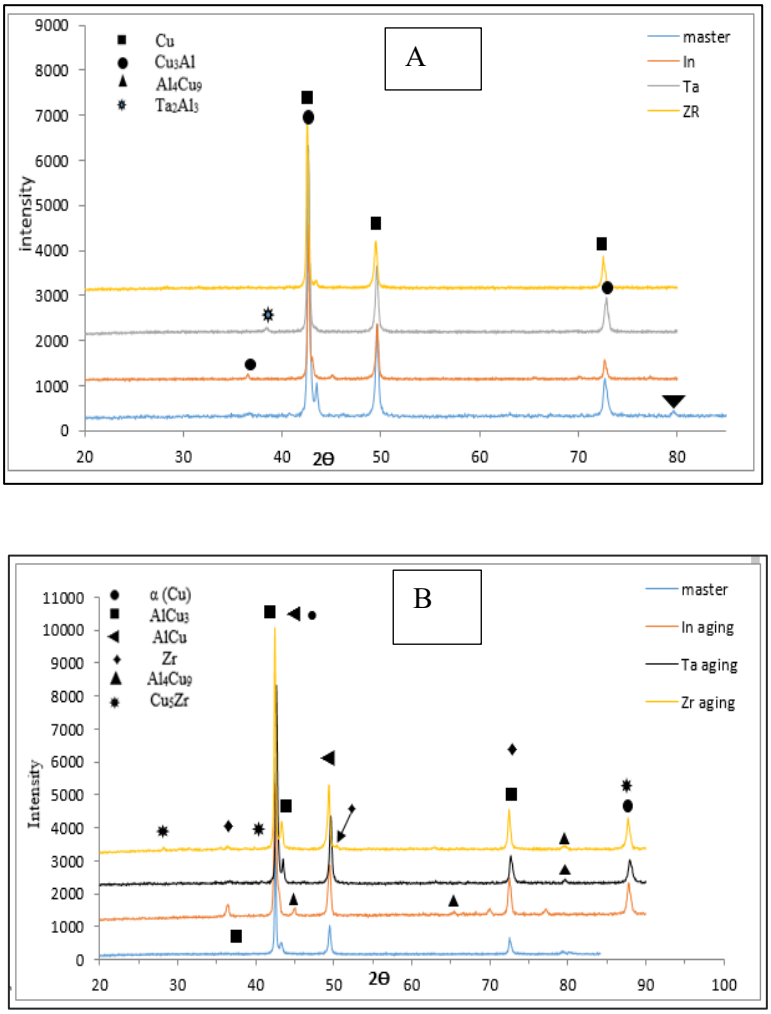

Figure 4 (A and B): XRD after sintering and quenching.

3.2 Open Circuit Potential

For any closed electrical circuit, anodic and cathodic reactions take place. The sample was placed in a corrosive solution, then a reaction occurred between the surface of the sample and the corrosive medium. This resulted in a potential called the 'open circuit potential'. The forming and breaking of the protective oxide layer were observed due to the potential curve rise and fall that was acquired during the test period. The stability in the potential value is reached (the potential value is fixed) when the anode reaction is equal to the cathodic reaction or the oxidation reaction is equal to the reduction reaction, and therefore, the free energy is equal to zero. The open circuit potential of the CuAlMn (master alloys) with and without additions three % wt. (Ta, Zr and In) is represented in Figure 5. There is a difference between the potential corrosion readings of the CuAlMn alloy and the CuAlMnZr, CuAlMnTa, CuAlMnIn alloys. This means that the alloy shows more nobility when these additions are added. From Figure 5, the CuAlMnIn alloy shows the lowest potential corrosion value. The result of the potential towards more negativity with time means that insufficient oxide layer has formed to prevent the corrosion.

.

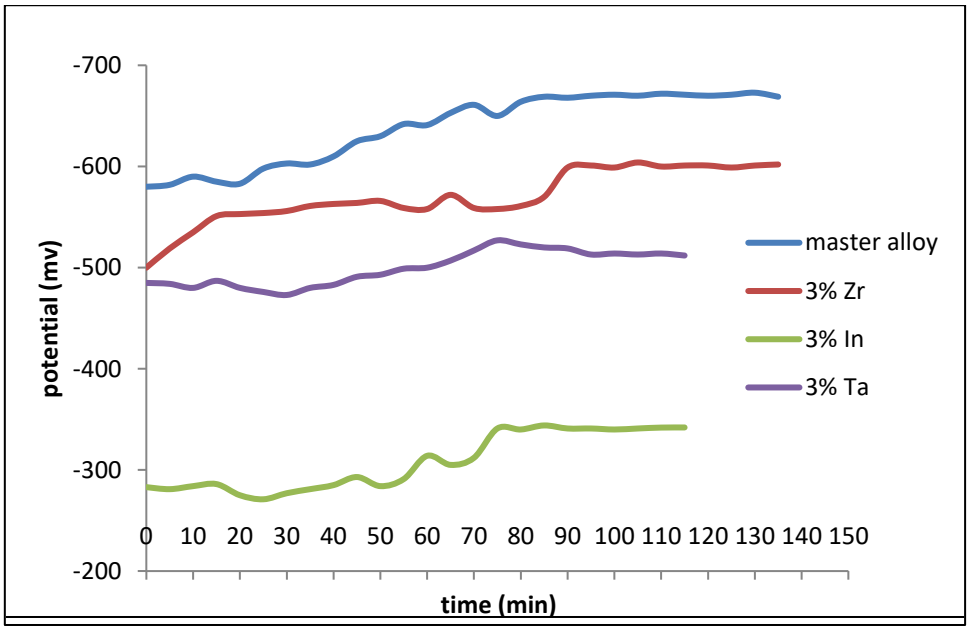

Figure 5: Open circuit potential of samples in 3.5 % NaCl.

3.3. Potential-dynamic polarisation

The potential-dynamic polarisation curve is normally illustrated in a semi logarithm chart comprising cathodic and anodic sections, which represent the effects of the electro-chemical reactions between the sample and corrosion solution. The reaction of the hydrogen evolution is called a cathodic reaction or the reduction of oxygen, and the oxidation reaction is called an anodic reaction or the corrosion process of the alloy. The polarisation curves of the base CuAlMn and CuAlMn-X (x = Ta, Zr and In) SMAs are explained in Fig 6. The corrosion potential (Ecorre) and corrosion current density ($i$corre) samples are presented in Table 5. The addition of Ta, Zr and In to the base CAM improved the C.R value. The curves clearly indicate that the lowest corrosion rate is attributed to CuAlMn-3Ta. The high concentration of the Ta and In ions in the corrosion product film means that it has low solubility in an aggressive chloride-containing solution [22, 23].

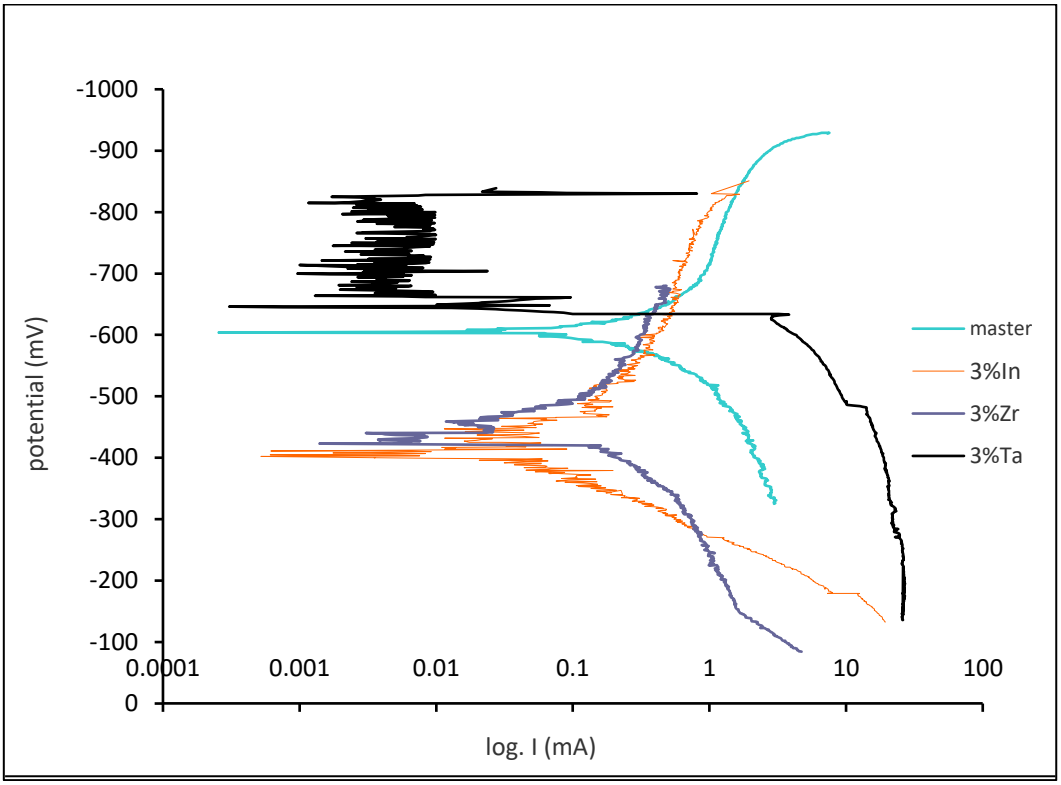

Figure 6: Potential-dynamic polarisation curve for CuAlMn alloy in the aging state in 3.5 % NaCl.

Table 3: Electrochemical parameters of ternary Cu-Al-Mn and quaternary SMAs in the 3.5 wt.% NaCl solution that was obtained from the polarisation test.

Alloys	Current density Icorr (μA / cm2)	Potential *E*corr (mV versus SCE)	Corrosion rate $C.R$ (mm / year)	Cathodic slope, βC (mV / decade) versus SCE	Anodic slope, βa (mV / decade) versus SCE
CuAlMn	156.74	-528.5	3.85	-65.9	72.8
CuAlMnTa	13.41	-430.6	0.306	-55.1	72
CuAlMnZr	35.87	-458.2	0.819	-80.5	66.1
CuAlMnIn	3.42	-643.6	0.078	-11.2	18.8

3.4. Optical Microstructures (OM)

The optical microstructures of the CuAlMn samples with quaternary additions is given in Figure 7. At the betatisation at 900 °C, the CuAlMn alloy had a disordered β phase with a body centre cubic structure. After solution annealing at 900 °C and quenching in ice water, the structure consisted of the β_1' martensite and β parent phase at room temperature [27]. The formation of the martensitic is clearly seen in the quenched samples (austenite phase completes the transformation to martensite phase). As seen in Figure 8, all the samples are formed from the

complete lath-type martensitic structure with thin martensitic plates or variants. The martensite variants have different orientations in each grain. These martensite variants are known as lath types. A β m̀artensite with thick plates was observed in these alloys and needle-type martensites [24–26]

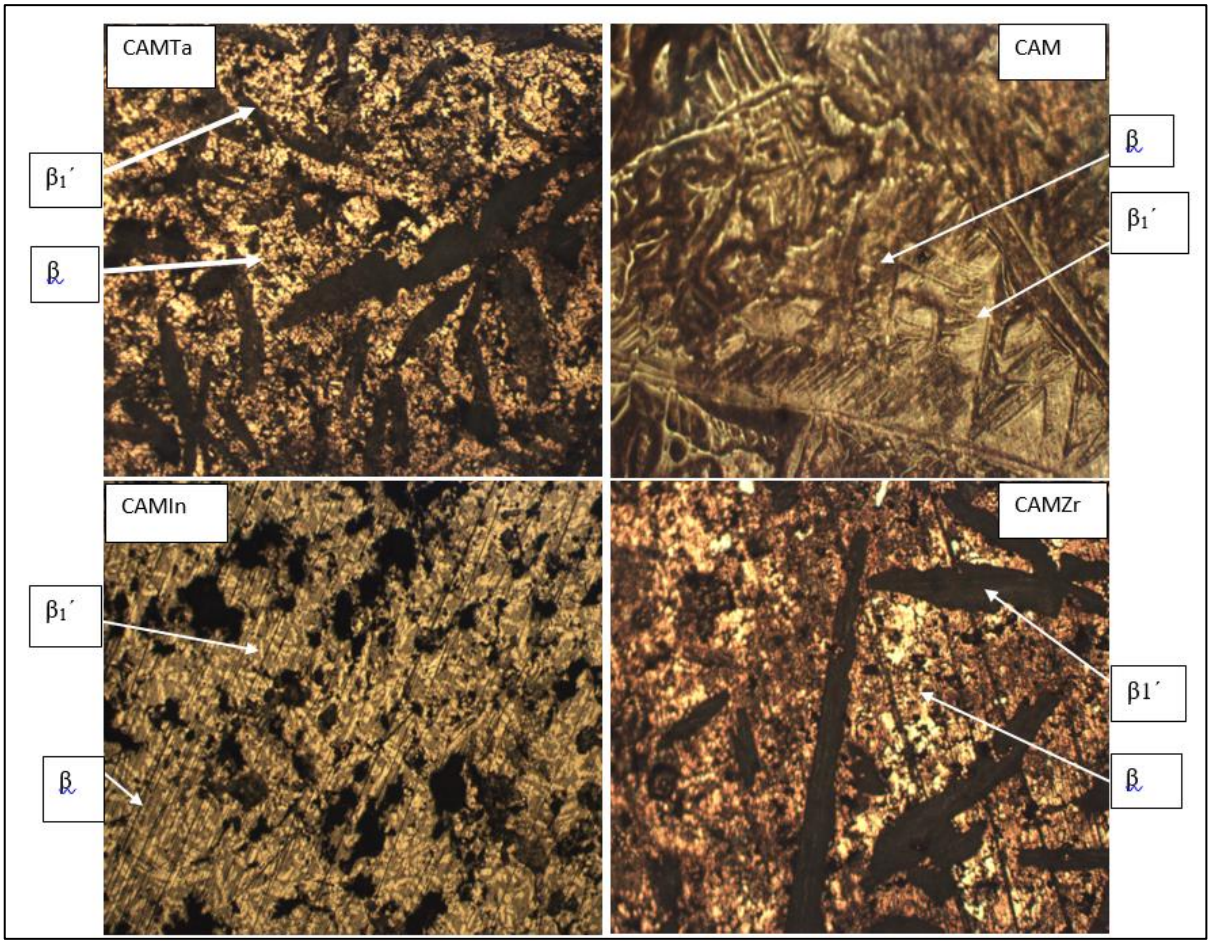

Figure 7: Optical micrographs of CuAlMn SMAs with quaternary alloying addition (100µm).

3.5. Micro Hardness Result

Figure 8 shows the micro hardness of Cu8Al9Mn SMA with and without the addition of three wt.% Ta, Zr and In. Each reading represents an average of four readings. This changes into a micro hardness value once Zr, Ta and In are added. It may act as a grain refinement and presence of intermetallic compounds as Cu5Zr and Ta2Al3 are at the grain boundaries of the alloys and dissolution of the elements in the alloy matrix. This result matches with Raied Z. and Safaa N [21, 28].

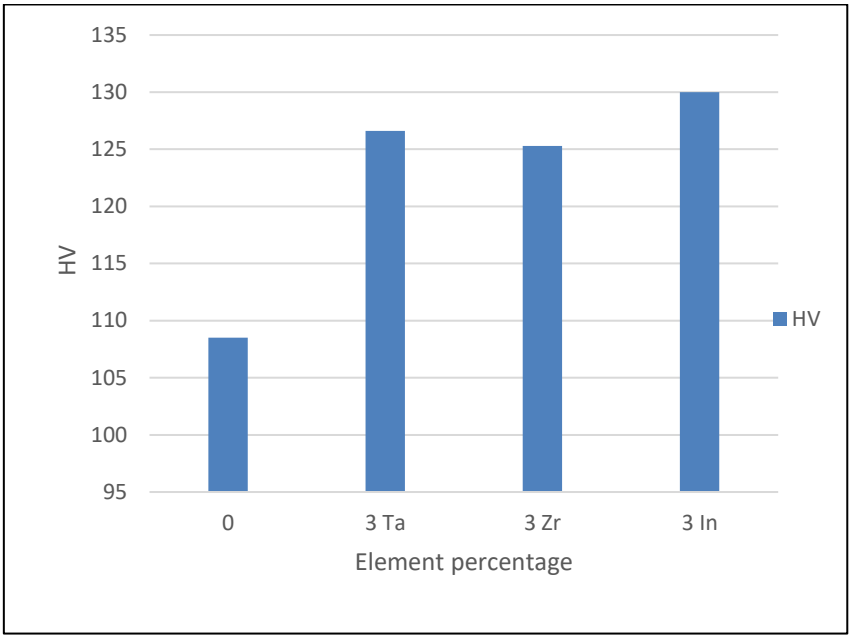

Figure 8: Micro hardness of CuAlMn SMAs.

4. Conclusion

In the corrosion results, we noticed that CuAlMnIn had the lowest corrosion potential, whereas CuAlMnTa had the best corrosion resistance (97.8 %) compared to the master alloy. We also noticed that the appearance of the passive and trance-passive region indicated that the metal gained a protective oxide layer coating. The microstructure results exposed that the addition of a fourth element three wt.% (Ta, Zr and In) can reduce the grain's size of ternary Cu eight % Al nine % Mn SMAs, whereas the In was the best grain refiner. The XRD analysis showed that the types of martensite that were formed were 18R (β᾽Cu3Al) and a small amount of γ᾽ martensite with a thick plate shape. It was observed that the hardness of the master alloy (Cu eight Al nine Mn) shape memory alloy was improved by adding Ta, Zr and In.

References

[1] Safaa N. Sauda, E. Hamzaha, T. Abubakar and RahelehS 2013 A Review on Influence of Alloying Elements on the Microstructure and Mechanical Properties of Cu-Al-Ni Shape Memory Alloys *Jurnal Teknologi (Sciences & Engineering)* **64:1** 51–56.

[2] Mirko G., Stjepan K., Ivana I., Magdalena S., Tamara H., Borut K., Diana Ć. and Omer B. 2017 Microstructural characterization of Cu82.3Al8.3Mn9.4 shape memory alloy after rolling *Metallurgical and Materials Engineering.*

[3] Canan C., Ayşe T. and İskender Özkul, 2017 Fabrication of CuAlNi shape memory alloy thine film by evaporation Turkish *Journal of Engineering (TUJE)* **1** 2 70-75.

[4] Zhenghua Denga, Haiqing Yina,b,, Cong Zhanga,b, Guofei Zhanga, Tong Zhangc, ZiKui Liud, Haibao Wange and Xuanhui Qua 2019 Sintering mechanism of Cu-9Al alloy prepared from elemental powders *Natural Science: Materials International* 29 425–431.

[5] S. Montecinos A., R. Romero and M. Stipcich 2015 Grain size evolution in Cu-based shape memory alloys J *Mater Sci* 50 3994–4002.

[6] Uwe A., Hennadiy Z., Bernd. and Werner R. 2018 Impact of Alloy Composition and Thermal Stabilization on Martensitic Phase Transformation Structures in CuAlMn Shape Memory Alloys *Materials Research* 21 **2**.

[7] Emine A. and Ilhan A. 2014 Effects of Heat Treatment and Deformation on 2H and 18R Martensites in Cu–9.97%Al–4.62%Mn Alloy, *Arab J Sci Eng* **39**:575–580.

[8] Rupa D., Ashish J., Shahadat H., Abhishek P and V. Sampath 2018 Effect of Alloying Additions on the Properties Affecting Shape Memory Properties of Cu–12.5Al–5Mn Alloy *Research and Technology* 377-390.

[9] Guofei Z., Haiqing Y., Cong Z., Zhenghua D., Ruijie Z., Xue J. and Xuanhui Q. 2020 Effect of Mn on microstructure and properties of Cu-12Al powder metallurgy alloy *Mater. Res. Express* 7 016546.

[10] Sampath, V., and U. S. Mallik 2009 Influence of minor additions of boron and zirconium on shape memory properties and grain refinement of a Cu-Al-Mn shape memory alloy European *Symposium on Martensitic Transformation. EDP Science* 7.

[11] Canan Aksu, Canbay and Tercan Polat 2017 Thermal and structural alternations in CuAlMnNi shape memory alloy by the effect of different pressure applications Physica B **521** 331–338

[12] T. Omori, N. Koeda, Y. Sutou, R. Kainuma, K. Ishida 2007 Superplasticity of Cu-Al-MnNi shape memory alloy Mater. Trans. **11** 2914–2918.

[13] Y. Sutou, N. Koeda, T. Omori, R. Kainuma and K. Ishida 2009 Effects of ageing on bainitic and thermally induced martensitic transformations in ductile Cu-Al-Mn based shape memory alloys Acta Mater. **57** 5748–5758.

[14] Kainuma, S. Takahashi and K. Ishida 1996 Thermoelastic martensite and shape memory effect in ductile Cu-Al-Mn alloys *Metal Mater. Trans.* **27** 2187–2195.

[15] C. Aksu Canbay and Z. Karagoz 2013 The effect of quaternary element on the thermodynamic parameters and structure of CuAlMn shape memory alloys *Physica B* **521** 331-338

[16] Ghulam Gohar, Tareq M. and Asad Shah 2017 Investigation of thermal and mechanical properties of Cu-Al alloys with silver addition prepared by powder metallurgy *Journal of Alloys and Compounds* 11.176

[17] Zhiming S., Ming L. and Andrej A. 2010 Measurement of the corrosion rate of magnesium alloys using Tafel extrapolation *Corrosion Science* **52** 579–588.

[18] Shuiyuan Y., Fan Z., Jialin Wu, Yong Lu, Zhan Shi, Cuiping W., and Xingjun L. 2017 Superelasticity and shape memory effect in Cu–Al–Mn–V shape memory alloys Materials *and Design* **115** 17–25.

[19] C. Pilz , E. Matsumura , A. Paganotti , Cornejo and R. Silva 2020 Microstructure and phase stability of CuAlMnAgZr multicomponent alloys *Materials Chemistry and Physics* **241** 122343.

[20] Raied Z. Alfay, Ayad M. Takhakh and Abdul Raheem K. 2013 Effect of Ta addition on hardness and wear resist of Cu-Al-Ni shape memory alloy fabricated by powder metallurgy *IEEE Business Engineering and Industrial Applications Colloquium (BEIAC)*.

[21] H.-J. Lee, E. Akiyama, H. Habazaki, A. Kawashima, K. Asami and K. Hashimoto 1997 The roles of tantalum and phosphorus in the corrosion behavior of Ni-Ta-P alloys in 12MHCl *Corrosion Science* **39** 2 321–332.

[22] J. Bhattarai, E. Akiyama, H. Habazaki, A. Kawashima, K. Asami, and K.Hashimoto 1998 The passivation behavior of sputter deposited W-Ta alloys in 12 M HCl *Corrosion Science* **40** 4-5 757–779.

[23] Y. Jiao, Y. Wena, N. Lia, J. Hea and J. Tenga 2010 Effect of solution treatment on damping capacity and shape memory effect of a CuAlMn alloy *Journal of Alloys and Compounds* **491** 627–630.

[24] U. Mallik and V. Sampath 2009 Influence of quaternary alloying additions on transformation temperatures and shape memory properties of Cu–Al–Mn shape memory alloy *Journal of Alloys and Compounds* **469** 156–163.

[25] Safaa N., Esah H., Tuty Abu bakar, Mustafa K., and Abdollah B. 2015 Effect of a fourth alloying element on the microstructure and mechanical properties of Cu–Al–Ni shape memory alloys *Materials Research Society 30* 14.

[26] C. Aksu and A. Keskin 2014 Effects of vanadium and cadmium on transformation temperatures of Cu–Al–Mn shape memory alloy *Journal of Thermal Analysis and Calorimetry (JTAC)* **118**, pages1407–1412

[27] S. Kožuh, M. Gojić, I. Ivanić, T. Holjevac Grgurić, B. Kosec, and I. Anžel 2018 The Effect of Heat Treatment on the Microstructure and Mechanical Properties of Cu-Al-Mn Shape Memory Alloy *KUI* **67** 1-2. https://hrcak.srce.hr/file/284196

[28] Safaa N. Saud,1 E. Hamzah, H. R. Bakhsheshi-Rad, and T. Abubakar 2017 Effect of Ta Additions on the Microstructure Damping and Shape Memory behaviors of Pre alloyed Cu-Al-Ni Shape Memory Alloys *Hindawi* **2017** 13.